Catalysis Today 146 (2009) 37–43

Contents lists available at ScienceDirect

Catalysis Today

journal homepage: www.elsevier.com/locate/cattod

Effective and stable bioethanol steam reforming catalyst based on Ni and Co supported on all-silica delaminated ITQ-2 zeolite

Antonio Chica *, Salvador Sayas

Instituto de Tecnología Química, UPV-CSIC, Avda. de los Naranjos s/n, 46022 Valencia, Spain

ARTICLE INFO

Article history:
Available online 31 January 2009

Keywords:
Bioethanol
Steam reforming
Nickel
Cobalt
ITQ-2
SiO_2

ABSTRACT

Catalysts based on Ni and Co supported on pure silica ITQ-2 delaminated zeolite have been prepared and tested in the bioethanol steam reforming. Ni/ITQ-2 zeolite was found the most active material while ITQ-2 zeolite containing Co exhibited the highest hydrogen selectivity and the lowest CO selectivity. Deposition of coke occurs in both materials; however, deactivation was not detected during the experimentation time (72 h). The particular structure and physico-chemical characteristics of the ITQ-2 zeolite as support [absence of acid sites, high external surface area (>800 $m^2\ g^{-1}$)] could account for the high activity, selectivity and stability detected.

1. Introduction

The scarcity of fossil fuels, the rising of their price and the world contamination problems associated with them make it necessary to develop renewable and cleaned energy alternatives independent of fossil fuels. Among alternative fuels, hydrogen could be a viable option because it exhibits the greatest heating value (39.4 kWh/kg) of all chemical fuels. Its combustion to heat or power is simple and clean. When combusted with oxygen hydrogen forms water and no pollutants are emitted. Unfortunately, it is not freely available in nature and it must be produced by some means.

About 95% of the hydrogen we use today comes from reforming of natural gas. But to realize the full benefits of a hydrogen economy-sustainability, increased energy security, diverse energy supply and reduced air pollution, hydrogen must be produced cleanly and efficiently from available renewable resources. Hydrogen can be produced from biomass, a removable and CO_2-neutral energy source with respect to the green house effect [1–3]. Because biomass consumes atmospheric carbon dioxide (CO_2) during growth, it can have a small net CO_2 impact compared with fossil fuels.

Reforming of renewable biomass feedstocks [4], such as bioethanol, has become an important and active research area in view of hydrogen production. In comparison with other fuels, bioethanol presents a series of advantages, since it is easier to store, handle and transport in a safe way due to its lower toxicity and volatility. In addition, from the environmental point of view, bioethanol presents important advantages since it is metal-free and does not release pollutant gases (SO_x, NO_x and others).

The ethanol obtained from biomass fermentation, also called bioethanol, is an aqueous solution containing ethanol in the ranges from 10% to 18% [5]. The presence of this amount of water represents an important advantage from the point of view of the steam reforming process because the water necessary to carry out the reaction is already contained in the raw bioethanol. Thus, it will not be required to carry out additional distillation steps that means, from the industrial standpoint, a substantial economic and energetic saving.

Although bioethanol seems to be a promising fuel to produce hydrogen, the amount of published studies on the reforming of ethanol is lower than that on hydrocarbons or methanol. Several reviews about the development of catalysts applied to ethanol steam reforming have been published lately [6–9]. Catalytic materials such as metallic oxides (ZnO, MgO, V_2O_5, Al_2O_3, TiO_2, La_2O_3, CeO_2, SmO_3) [10–12], supported metals (Co/Al_2O_3, Co/La_2O_3, Co/SiO_2, Co/MgO, Co/ZrO_2, Co–ZnO, Co/TiO_2, Co/V_2O_5, Co/CeO_2, Co/Sm_2O_3, Co/CeO_2–ZrO_2, Co/C, Ni/La_2O_3, $Ni/(La_2O_3$–$Al_2O_3)$, Ni/Al_2O_3, Ni/MgO, Ni–Cu/SiO_2, Ni–Cu/Al_2O_3, Ni–Cu–K/Al_2O_3) [13–24] and precious metals supported on oxides (Rh/TiO_2, Rh/SiO_2, Rh/CeO_2, Rh/ZrO_2, Rh/Al_2O_3, Rh/MgO, Rh/Al_2O_3, Rh/CeO_2–ZrO_2, Rh–Au/CeO_2, Rh–Pt/CeO_2, Pd/CeO_2, Pt/CeO_2, Au/CeO_2, Pd/Al_2O_3, Pt–Pd/CeO_2) [25–38] are reported in these reviews.

Thermodynamic analyses have shown that a high conversion of ethanol to hydrogen is possible above 250 °C and also that the high water/ethanol molar ratio of raw bioethanol is beneficial to

* Corresponding author. Tel.: +34 963877000x78508; fax: +34 963877809.
E-mail address: achica@itq.upv.es (A. Chica).

0920-5861/$ – see front matter © 2009 Elsevier B.V. All rights reserved.
doi:10.1016/j.cattod.2008.12.024

Table 1
Some of the reactions that occur during the steam reforming of bioethanol.

Reaction	Equation
Reforming with excess of water	$CH_3CH_2OH + 3H_2O \rightarrow 2CO_2 + 6H_2$
Reforming with deficit of water	$CH_3CH_2OH + H_2O \rightarrow 2CO + 4H_2$ $CH_3CH_2OH + 2H_2 \rightarrow 2CH_4 + H_2O$
Dehydrogenation	$CH_3CH_2OH \rightarrow C_2H_4O+H_2$
Acetaldehyde decomposition	$C_2H_4O \rightarrow CH_4 + CO$
Acetaldehyde reforming	$C_2H_4O + H_2O \rightarrow 3H_2 + 2CO$
Dehydration	$CH_3CH_2OH \rightarrow C_2H_4 + H_2O$
Coke formation	$C_2H_4 \rightarrow$ polymeric deposits (coke)
Decomposition	$CH_3CH_2OH \rightarrow CO + CH_4 + H_2$ $2CH_3CH_2OH \rightarrow C_3H_6O + CO + 3H_2$ $CH_3CH_2OH \rightarrow 0.5CO_2 + 1.5\ CH_4$
Methanation	$CO + 3H_2 \rightarrow CH_4 + H_2O$ $CO_2 + 4H_2 \rightarrow CH_4 + 2H_2O$
Decomposition of methane	$CH_4 \rightarrow 2H_2 + C$
Boudouard reaction	$2CO \rightarrow CO_2 + C$
Water gas shift reaction	$CO + H_2O \rightarrow CO_2 + H_2$

increase hydrogen yield and to decrease the formation of by-products such as methane and carbon monoxide, and carbon deposition. Table 1 shows a summary of the possible reaction pathways follows by the ethanol during its catalytic steam reforming. The extension in which each reaction takes place over the catalyst will depend on the nature of metal, type of precursor, preparation method, type of support, presence of additives, and operating conditions.

Despite the enormous efforts that are being undertaken in the development of efficient catalysts for the steam reforming of ethanol, there are still major constraints affecting the proper functioning of the catalyst and the generation of a "clean" hydrogen that can be used directly in fuel cells. Ethanol reforming process, besides the formation of H_2, produced high levels of CO, which is a strong poison for the hydrogen oxidation reaction taking place on the anode of fuel cell. Even with more advanced anode catalysts, the system cannot accept more than 100 ppm for efficient operation [39]. In addition other undesirable products such as CH_4 are produced. For that reason a high-quality ethanol steam reforming catalyst should work at low temperatures in order to promote the WGS reaction, which consumes CO to produce hydrogen. Methanation reaction should also be inhibited since it consumes hydrogen. Coke formation and metal sintering are also serious obstacles for the stable operation of the steam reforming catalysts. As it can be seen in Table 1 the formation of coke is related to the formation of ethylene and its subsequent polymerization. Therefore, the reforming catalysts should avoid the dehydration of ethanol and subsequent formation of ethylene [40]. If the formation of the ethylene could not be avoided the reforming catalysts should be able to reform it efficiently.

Activity of the steam reforming catalyst can be increased achieving a good dispersion of metallic sites on the support while coke formation could decrease using non-acidic supports that would avoid the ethanol dehydration reaction. Thus, it is clear that the support plays an important role in steam reforming activity since it can help to improve the dispersion of metal catalyst enhancing the metal catalyst activity via metal-support interactions [6] and avoiding the metal sinterization. Recently, a new zeolitic material, ITQ-2, has been synthesized in our laboratories [41]. The delaminated zeolite consists of thin sheets of 2.5 nm in height presenting a hexagonal array of "cups" (0.7 nm × 0.7 nm) that penetrate into the sheet from both sides connected by a double 6-member ring (MR) window (Fig. 1). The singular structure of this delaminated zeolite, and particularly the very high and well-defined external surface area, makes these materials very attractive to be used as supports for dispersing active metal phases. In this sense, NiMo, Pt, and Co catalysts supported on (Al)-ITQ-2 and all-silica were applied for hydrocracking of vacuum gas oil, hydrogenation of aromatics compounds and Fischer–Tropsch reaction, respectively, with promising results [42,43]. For that reason, in this work we have studied the possibilities of using pure silica (non-acidic) delaminated ITQ-2 zeolite as support for preparing Ni- and Co-based steam reforming catalysts.

2. Experimental

2.1. Preparation of catalysts

Pure silica ITQ-2 zeolite was obtained by swelling the layered MWW zeolite precursor in cetyltrimethylammonium bromide (CTABr) as described in [41]. Typically, 27 g of precursor is mixed with 105 g of an aqueous solution of CTABr (29 wt%) and 33 g of an aqueous solution of tetrapropylammoniumhydroxide (TPAOH, 40 wt%), and the resulting solution is refluxed for 16 h at 353 K. The layers are forced apart by placing the slurry in an ultrasound bath (50 W, 40 kHz) for 1 h. Separation of the solids is done by the acidification of the medium with concentrated hydrochloric acid (HCl, 37%) until the pH is below 2, followed by centrifugation. Calcination of the material at 813 K yields all-silica ITQ-2 zeolite.

For comparison purposes a commercial amorphous SiO_2 (Fluka, silica gel 100) was also used as Co and Ni support.

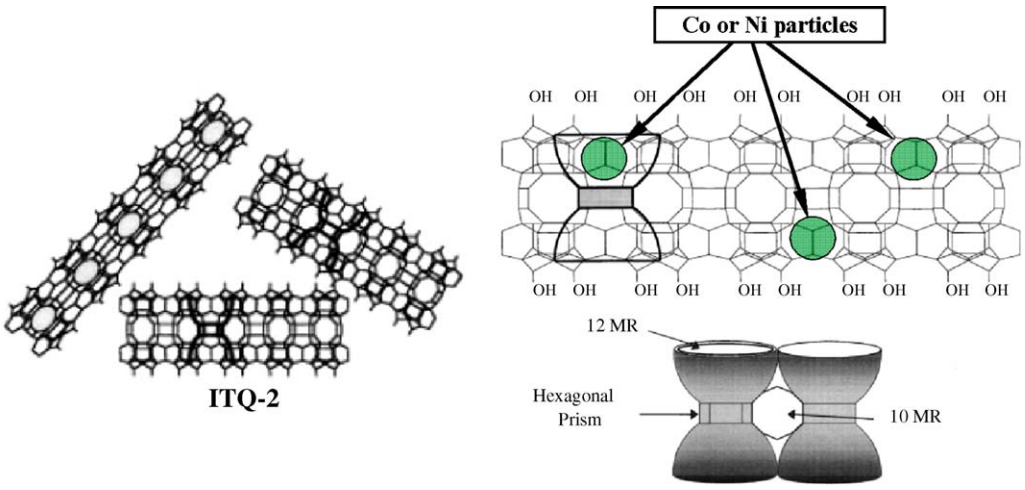

Fig. 1. Schematic representation of the ITQ-2 structure.

Incorporation of Co and Ni was accomplished by incipient wetness impregnation with an aqueous solution containing the required amount of $Co(NO_3)_2{\cdot}6H_2O$ (Aldrich, 98%) and $Ni(NO_3)_2{\cdot}6H_2O$ (Fluka, 98.5%) to achieve a nominal concentration of 20 wt% of metal in the final catalysts. The solid was further dried at room temperature for 16 h. Finally, Co/ITQ-2, Ni/ITQ-2, Co/SiO_2, and Ni/SiO_2 catalysts were calcined in muffle oven at 873 K for 3 h.

2.2. Characterization techniques

The cobalt and nickel content in the calcined samples was determined by atomic absorption spectrophotometry (AAS) in a Varian Spectra A-l0 Plus apparatus.

Textural properties of the ITQ-2 and SiO_2 pattern and Co- and Ni-containing samples were obtained from the nitrogen adsorption isotherms determined at 77 K in a Micromeritics ASAP 2000 equipment. Surface areas were calculated by the BET method and the pore-size distributions were obtained using the BJH formalism. Prior to the adsorption measurements the samples were outgassed at 473 K for 24 h.

X-ray diffraction was used to identify the nature of the crystalline cobalt and nickel oxide phases. XRD patterns were obtained at room temperature in a Philips X'pert diffractometer using monochromatized CuKα radiation.

The reduction behaviour of the supported oxidized cobalt and nickel phases was studied by temperature-programmed reduction (TPR) in a Micromeritics Autochem 2910 equipment. About 50 mg of the calcined catalyst was initially flushed with 30 cm^3/min of Ar at room temperature for 30 min and then a mixture of 10 vol% of H_2 in Ar was passed through the catalyst at a total flow rate of 50 cm^3/min while the temperature is increased up to 1173 K at a heating rate of 10 K/min. The H_2 consumption rate was monitored in a thermal conductivity detector (TCD) previously calibrated using the reduction of CuO as reference. The degree of reduction was determined from TPR experiments comparing the total amount of hydrogen consumed by each catalyst and the amount of hydrogen theoretically necessary to complete the reduction of Co_3O_4 and NiO oxide species present in the catalyst.

The metallic particle size was estimated from H_2 adsorption using the double isotherm method on a Quantachrome Autosorb-1 equipment. Prior to adsorption, the samples were reduced in situ in flowing hydrogen at the same reduction temperature applied before catalysis. After reduction, the samples were degassed at 1333×10^{-3} Pa for 2 h at the reduction temperature, and the temperature lowered to 313 K. Then, pure H_2 was admitted and the first adsorption isotherm was measured. After evacuation at 313 K, the second isotherm was measured. The amount of chemisorbed hydrogen was then obtained by subtracting the two isotherms. The average Pt particle sizes were estimated from the metal's surface area assuming a spherical geometry.

The amount of carbon deposited in the catalysts after steam reforming reaction was determined by elemental analysis using a Carlo Erba 1106 analyzer.

2.3. Catalytic study

Steam reforming experiments were carried out in a continuous fixed bed reactor at atmospheric pressure, H_2O/EtOH molar ratio of 13, GHSV 4700 h^{-1} and a range of temperatures between 573 K and 873 K. Before reaction the catalysts were reduced "in situ" in flow of H_2 (1.67 $cm^3\ s^{-1}$) at 873 K for 2 h.

In a typical catalytic test the reactor was loaded with 0.15 g of catalyst (grain-size: 0.25–0.42 mm), diluted with 3 g of carborundum (SiC) (grain-size: 0.60–0.80 mm), The water/ethanol mixture was fed from a pressurized container using a liquid flow controller (Bronkhorst), and vaporized at 473 K into a stream of nitrogen. The total gas flow was 2 $cm^3\ s^{-1}$ (83.7 vol% N_2).

The analysis of the compounds of reaction was carried out on-line using a gas chromatograph (Varian 3800) equipped with two columns (TRB-5, L = 30 m, DI = 0.25 mm; CarboSieve SII, L = 3 m, DI = 2.1 mm) and two detectors, a thermal conductivity and flame ionization (FID).

The bioethanol conversion and selectivity to the different reaction products were determined according to the Eqs. (1) and (2), where $(F_{EtOH})_O$ is the flow of ethanol fed to the reactor (mol s^{-1}), $(F_{EtOH})_f$ the flow of ethanol that comes from the reactor and F_j the flow of product j that comes from the reactor. Selectivity values were calculated as the molar percentage of the products obtained, excluding water.

$$X(\%, \text{mol}) = \frac{(F_{EtOH})_o - (F_{EtOH})_f}{(F_{EtOH})_o} \times 100 \quad (1)$$

$$S(\%, \text{mol}) = \frac{F_j}{(\sum F_j)_{\text{products}}} \times 100 \quad (2)$$

3. Results and discussion

3.1. Characterization

X-ray diffraction patterns of calcined ITQ-2 are showed in Fig. 2. As it can be seen calcined ITQ-2 sample does not show the 0 0 *l* peaks with the 2.5-nm periodicity typical of the MWW topology, indicating a reduction in long-range order along the *c* axis. These structural changes are in agreement with the proposed structure (Fig. 1) in which the ITQ-2 material is mostly formed by single layers of the corresponding lamellar precursors.

The textural properties of the ITQ-2 and SiO_2 pattern derived from the N_2 adsorption isotherms are summarized in Table 2. As observed, ITQ-2 presents a high BET surface area (835 m^2/g) and total pore volume (0.77 $cm^3\ g^{-1}$). Textural properties of the Co- and Ni-containing catalysts are also given in Table 1. A reduction in surface area and pore volume is noted for all samples after incorporation of cobalt and nickel (20 wt% Co and Ni). This loss of area can be explained assuming that cobalt and nickel in calcined samples are present in the form of Co_3O_4 and NiO, respectively, and that these phases do not contribute to the surface area. Thus, the incorporation of high level of cobalt and nickel (20 wt%) would lead to a dilution effect, which could explain the surface area reduction detected. Pore volume of the samples containing cobalt and nickel is also lower than in pattern materials. This indicates that a partial plugging of the support pores has also occurred after Co and Ni incorporation.

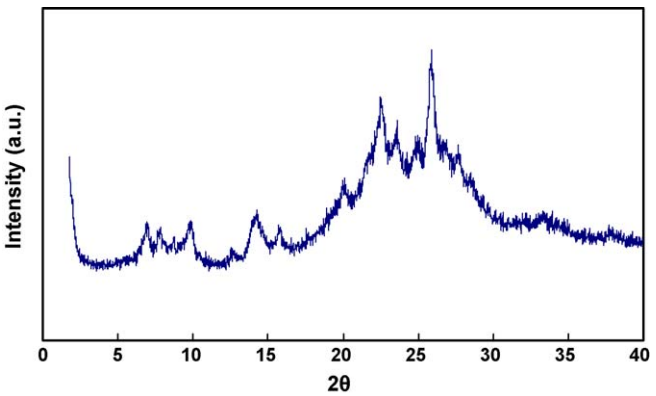

Fig. 2. X-ray diffraction pattern of calcined ITQ-2 zeolite.

Table 2
Metal content and textural properties of ITQ-2 and SiO_2 supports and metal-containing catalysts determined by nitrogen adsorption.

Catalyst	Metal content (wt%)	Surface area (BET) (m^2/g)	Pore volume (BJH) (cm^3/g)	Oxide particle size (XRD) (nm)	Metal particle size (H_2-chemisorption) (nm)
ITQ-2		835	0.77		
SiO_2		390	0.78		
Co/ITQ-2	20.1	507	0.54	15.9	9.6
Ni/ITQ-2	19.5	517	0.53	19.6	11.8
Co/SiO_2	19.8	258	0.54	21.3	17.1
Ni/SiO_2	20.1	245	0.55	29.8	24.3

The X-ray diffractograms (not shown) of the oxidized Co samples (Co/ITQ-2 and Co/SiO_2) exhibit the reflections at 2θ of about 31.3°, 36.9°, 45.0°, 59.4°, and 65.4° characteristic of the spinel Co_3O_4 phase, as it is usually observed for siliceous materials impregnated with cobalt nitrate precursor [44–46]. For Ni-containing materials (Ni/ITQ-2 and Ni/SiO_2) three reflexions appear at 2θ of about 37.5°, 44.7°, and 63° characteristic of the NiO cubic phase, as it is also usually observed for the siliceous material impregnated with nickel nitrate precursor [47,48].

For comparison purposes, the average diameters of the Co_3O_4 and NiO crystallites estimated from XRD patterns using the Scherrer equation [49] have been calculated as shown in Table 2. Particle size of Co_3O_4 and NiO supported on ITQ-2 material is found to be smaller than that supported on SiO_2.

The reduction behaviour of the supported cobalt and nickel oxide particles in the catalyst has been studied by TPR. The corresponding reduction curves are shown in Fig. 3. As observed, Co/ITQ-2 and Co/SiO_2 present two main reduction features with maxima at about 550 K and 590 K, which correspond to the two-step reduction process in which Co_3O_4 is first reduced to CoO and then CoO is reduced to Co°, as reported by different authors [46,50–52]. For Co/ITQ-2 sample the area of the second reduction peak (mean in a.u., Table 3) is larger than that for the Co/SiO_2. Additional broad diffuse hydrogen consumption between 680 K and 1050 K has been also observed for Co/ITQ-2 sample suggesting the existence of several cobalt species reducing at approximately the same temperature, which can be ascribed to the reduction of cobalt silicates probably formed by the reaction of highly dispersed CoO with the silica support during the reduction process [46,53,54].

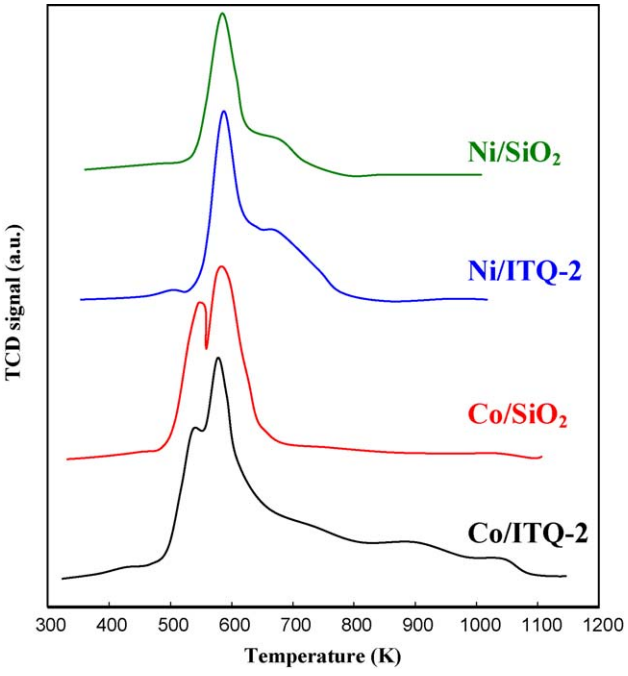

Fig. 3. TPR profiles of Co- and Ni-supported catalysts.

The TPR profile for the Ni-containing catalysts also presents two reduction peaks around 600 K, due to the reduction of Ni^{2+} [55,56], and around 680 K, which can be attributed to the formation of nickel silicate-type compounds owing to a strong Ni-support interaction [57]. The area of second reduction peak is also larger on Ni/ITQ-2 sample than that on Ni/SiO_2.

The reduction temperature and the peak width are indications of the degree of reduction and the level of interaction between different species, respectively. High reduction temperature indicates difficulty in reduction whereas broad peaks indicate a high degree of interaction between the species and the support [58]. Table 3 shows the reduction temperature and degree of reduction for cobalt and nickel supported on ITQ-2 and SiO_2. TPR results seem to indicate that cobalt and nickel oxides exhibit higher interaction with ITQ-2 support. In the case of Co/ITQ-2 the broad peak detected at higher temperatures (900–1050 K) suggests that a part of the cobalt species strongly interact with support causing difficulty in their reduction. Taking into account that the catalysts are reduced at 873 K before reaction it is possible that a part of the cobalt species in the ITQ-2 support remain in their oxidized form, thus, they would not participate in the bioethanol steam reforming. The low particle size determined by DRX for the cobalt oxide species supported on ITQ-2 material could also give explanation for the high reduction temperature displayed by part of the supported cobalt.

3.2. Catalytic activity

Fig. 4 shows the bioethanol conversion as a function of the reaction temperature. ITQ-2 samples containing Co and Ni exhibited higher bioethanol steam reforming activity than SiO_2 catalytic materials. On the other hand, Ni-based catalysts are more active at all temperature levels than their corresponding Co-based materials.

Catalytic activity of the cobalt- and nickel-supported catalysts was also compared at 573 K, H_2O/EtOH of 13, GHSV of 4700 h^{-1} and atmospheric pressure. The activity corresponding to the pseudo-stationary state (3–8 h on stream) is showed in Table 4. As it is observed ITQ-2 samples display the highest conversion levels. The global reaction rate determined as gram of bioethanol converted per gram of catalyst and per second is also presented

Table 3
TPR temperatures, peak areas and degree of reduction.

Catalyst	Temperature (K)		Area (a.u.)		Degree of reduction (%)
	Peak 1	Peak 2	Peak 1	Peak 2	
Co/ITQ-2	550	590	106	180	77.8
Ni/ITQ-2	600	680	120	60	87.9
Co/SiO_2	545	595	130	195	99.6
Ni/SiO_2	590	670	125	45	99.1

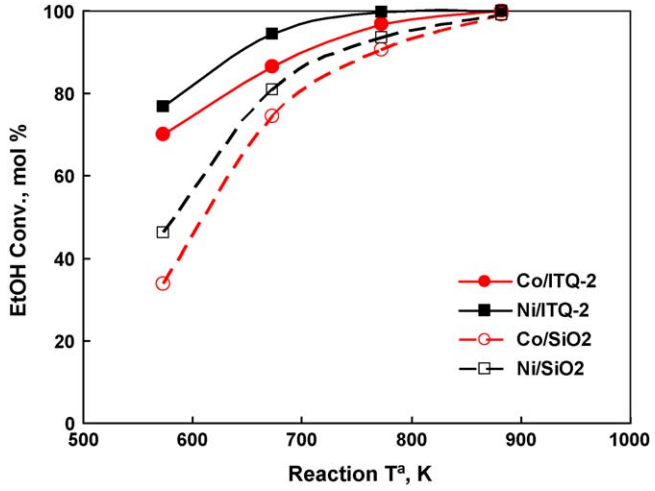

Fig. 4. Conversion of bioethanol versus reaction temperature. Reaction conditions: H_2O/bioEtOH = 13, GHSV = 4700 h^{-1} and atmospheric pressure.

in Table 4. Co/ITQ-2 and Ni/ITQ-2 show a reaction rate 2 times higher than that in Co/SiO_2 and Ni/SiO_2. The higher activity of the ITQ-2 samples can be attributed to the small Co and Ni particle size (see Table 2), resulting in a greater density of active surface metal size where the reforming of bioethanol can be carried out.

TOF has also been calculated as the moles of bioethanol converted per mol of reduced metal and per second. Mol of reduced metal was determined using the degree of reduction calculated for each catalyst (see Table 4). Turnover frequencies are quite different for ITQ-2 and SiO_2 support. The larger cobalt and nickel particle size determined by H_2-chemisorption (see Table 2) could explain the lower TOF of SiO_2 catalyst since in large metal particle size not all the active metal sites would be accessible for reaction. The lower Co and Ni metallic particle size detected for ITQ-2 support could be explained considering the particular structure of ITQ-2 zeolite formed by hexagonal array of "cups" (0.7 nm × 0.7 nm, see Fig. 1), which would provide an excellent position for the stabilization of the Ni or Co metal particles improving their dispersion, decreasing the metal particle size and avoiding their sinterization during reduction and reaction steps.

Table 4
Catalytic results for the bioethanol steam reforming on Co- and Ni-supported materials.

Catalyst	EtOH conversion (mol%)	Reaction rate[a] ($\times 10^{-2}$ s^{-1})	TOF[b] ($\times 10^{-2}$ s^{-1})
Co/ITQ-2	70.0	1.5	13.5
Ni/ITQ-2	76.8	1.6	12.1
Co/SiO_2	33.8	0.7	4.7
Ni/SiO_2	46.2	0.8	6.2

Reaction conditions: T^a = 573 K, H_2O/bioEtOH = 13, GHSV = 4700 h^{-1} and atmospheric pressure.

[a] Calculated as gram of bioethanol converted per gram of catalysts and per second.

[b] Calculated as mol of bioethanol converted per mol of reduced metal and per second. Mol of reduced metal was determined considering the degree of reduction: mol reduced metal = (total moles of metal × degree of reduction)/100.

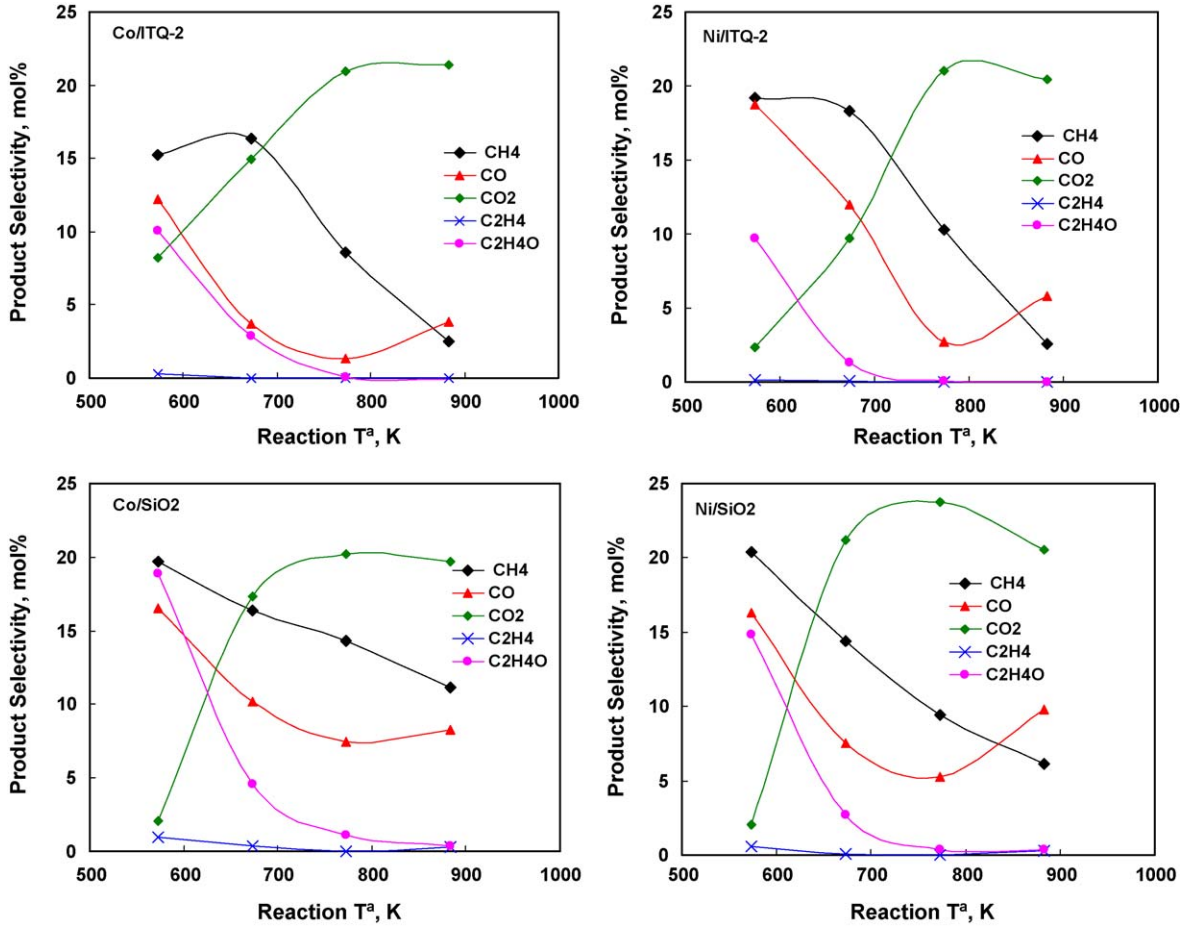

Fig. 5. Distribution of reaction products versus reaction temperature obtained in the steam reforming of bioethanol over Co- and Ni-supported on ITQ-2 and SiO_2. Reaction conditions: H_2O/bioEtOH = 13, GHSV = 4700 h^{-1} and atmospheric pressure.

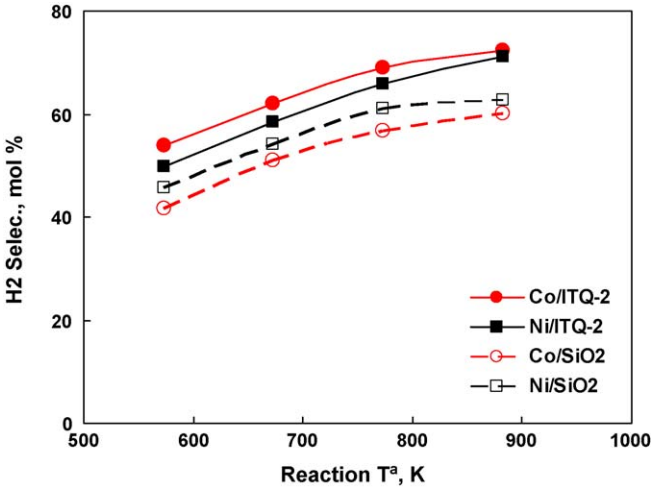

Fig. 6. Hydrogen selectivity versus reaction temperature obtained in the steam reforming of bioethanol over Co- and Ni-supported ITQ-2 and SiO_2. Reaction conditions: H_2O/bioEtOH = 13, GHSV = 4700 h^{-1} and atmospheric pressure.

Table 5
Catalytic activity of Co and Ni materials after 72 h of reaction time. Carbon content in the final catalyst is also showed in this table. Reaction conditions: H_2O/bioEtOH = 13, GHSV = 4700 h^{-1}, atmospheric pressure and 673 K.

Catalyst	EtOH conversion (mol%) (3 h)	EtOH conversion (mol%) (72 h)	Carbon content (wt%)
Co/ITQ-2	86.6	84.7	3.8
Ni/ITQ-2	94.3	93.6	3.1
Co/SiO_2	74.4	50.2	4.7
Ni/SiO_2	80.9	67.4	4.3

The products distribution obtained at four reaction temperatures (573, 673, 773 and 873 K) is shown in Fig. 5. The main observed products are H_2, CO_2, CH_4 and CO, but acetaldehyde, and ethane have also been detected at low reaction temperatures. As it is observed in Fig. 5 acetaldehyde is produced at low reaction temperatures in all the samples. The amount of produced acetaldehyde was larger in the samples using SiO_2 as support. On these catalysts traces of acetone were also detected. Above 773 K H_2, CO_2, CO and CH_4 are practically the only products and at 873 K these products approach equilibrium. At high temperature it can also be seen that Co/ITQ-2 exhibits the lowest CO selectivity as shown in Fig. 5.

The hydrogen selectivity and catalyst stability are the main parameters to be taken into account for practical use of the catalyst. The hydrogen selectivity with reaction temperature is shown in Fig. 6. The highest hydrogen yields are achieved at higher temperatures for all the catalysts being Co/ITQ-2 most selective to hydrogen.

Stability of these catalysts was also tested. It is well known that the stability of a steam reforming catalyst is strongly related to coke deposition and metal sintering. Table 5 shows the conversion of bioethanol after 72 h of reaction time for each catalyst at 673 K. As it can be seen deactivation was detected only for SiO_2 catalysts. However, elemental analysis of the catalysts after reaction shows the presence of coke in all the catalysts. Percentage of carbon is slightly larger for SiO_2 samples (see Table 5). This amount of carbon cannot explain the stronger deactivation exhibited by the SiO_2 materials. Together with the coke deposition it is possible that other effects such as metal sinterization account for the strong deactivation detected. In the case of ITQ-2 catalysts the high stability exhibited can be attributed firstly to the absence of acid sites in the pure silica ITQ-2 zeolite that can help to decrease the dehydration reaction that leads to the formation of ethylene and subsequent formation of coke. Secondly to their high external surface, which can provide a large surface for coke deposition and help to slow down the deactivation effects, and thirdly to the especial structure of ITQ-2 zeolite formed by hexagonal array of "cups" (0.7 nm × 0.7 nm, see Fig. 1), which can supply an excellent position for the stabilization of the Ni or Co metal particles improving their dispersion and preventing their agglomeration during the reduction and reaction stages.

Thus, the results here presented show that using pure silica delaminated ITQ-2 zeolite as support of Co and Ni can be prepared bioethanol steam reforming catalysts with higher activity and hydrogen selectivity, per mass of metal, and significant higher stability than that catalysts based on conventional amorphous silica.

4. Conclusions

A novel bioethanol steam reforming catalyst based on Ni or Co supported on pure silica ITQ-2 zeolite has been studied. The absence of acid sites on the pure silica ITQ-2 delaminated zeolite and its especial structure have allowed to prepared catalytic materials with high activity, selectivity and stability. These materials could be a good alternative to the current commercial reforming catalysts.

Acknowledgements

Financial support by the Polytechnic University of Valencia and Spanish Council for Scientific Research (CSIC) is gratefully acknowledged.

References

[1] D.K. Liguras, D.I. Kondarides, X.E. Verykios, Appl. Catal. B: Environ. 43 (2003) 345.
[2] G. Maggio, S. Freni, S. Cavallaro, J. Power Sources 74 (2001) 17.
[3] L.F. Brown, Int. J. Hydrogen Energy 26 (2001) 381.
[4] F. Ma, M.A. Hanna, Bioresour. Technol. 70 (1999) 1–15.
[5] S. Minteer, Alcoholic Fuels, Taylor & Francis, Boca Raton, 2006.
[6] P.D. Vaidya, A.E. Rodrigues, Chem. Eng. J. 117 (2006) 39.
[7] G. Kolios, B. Glöckler, A. Gritsch, A. Morillo, G. Eigenberger, Fuel Cells 5 (2005) 52.
[8] A. Haryanto, S. Fernando, N. Murali, S. Adhikari, Energy Fuels 19 (2005 2098).
[9] M. Meng, D.Y.C. Leung, M.K.H. Leung, Int. J. Hydrogen Energy 32 (2007) 3238.
[10] G.A. Deluga, J.R. Salge, L.D. Schmidt, X.E. Verykios, Science 303 (5660) (2004) 993.
[11] N.A. Fatsikostas, X.E. Verykios, J. Catal. 225 (2004) 439.
[12] J. Llorca, P.R. de la Piscina, J. Sales, N. Homs, Chem. Commun. (2001) 641.
[13] C. Diagne, H. Idriss, A. Kiennemann, Catal. Commun. 3 (2002) 565.
[14] J. Llorca, P.R. de la Piscina, J.A. Dalmon, J. Sales, N. Homs, Appl. Catal. B 43 (2003) 355.
[15] E. Vanhaecke, A.C. Roger, J.C. Vargas, A. Kiennemann, 1st European Hydrogen Energy Conference, September, Grenoble, France, (2003), p. 2.
[16] M.S. Batista, R.K.S. Santos, E.M. Assaf, J.M. Assaf, E.A. Ticianelli, J. Power Sources 134 (2004) 27.
[17] A. Kaddouri, C. Mazzocchia, Catal. Commun. 5 (2004) 339.
[18] J. Llorca, J.A. Dalmon, P.R. de la Piscina, N. Homs, Appl. Catal. A 243 (2003) 261.
[19] F. Haga, T. Nakajima, H. Miya, S. Mishima, Catal. Lett. 48 (1997) 223.
[20] H. Idriss, Platinum Met. Rev. 48 (2004) 105.
[21] J. Bussi, N. Bespalko, V. Veiga, A. Amaya, R. Faccio, M.C. Abello, Catal. Commun. 10 (2008) 33.
[22] G.B. Sun, K. Hidajat, X.S. Wu, S. Kawi, Appl. Catal. B 81 (2008) 303.
[23] E.B. Pereira, N. Homs, S. Marti, J.L.G. Fierro, P.R. de la, Piscina, J. Catal. 257 (2008) 206.
[24] H.V. Fajardo, L.F.D. Probst, N.L.V. Carreno, I.T.S. Garcia, A. Valentini, Catal. Lett. 119 (2007) 228.
[25] S. Cavallaro, Energy Fuels 14 (2000) 1195.
[26] M. Tóth, M. Dömök, J. Raskóx, A. Hancz, A. Erdohelyi, Presented in the Technical Program, May 16–19, Pisa, Italy, 2004.
[27] V. Fierro, V. Klouz, O. Akdim, C. Mirodatos, Catal. Today 75 (2002) 141.
[28] S. Velu, N. Satoh, C.S. Gopinath, K. Suzuki, Catal. Lett. 82 (2002) 145.
[29] M.A. Goula, S.K. Kontou, P.E. Tsiakaras, Appl. Catal. B 49 (2004) 135.
[30] P. Sheng, H. Idriss, J. Vac. Sci. Technol. A 22 (2004) 1652.
[31] D. Srinivas, C.V.V. Satyanarayana, H.S. Potdar, P. Ratnasamy, Appl. Catal. A 246 (2003) 323.
[32] N.R.C.F. Machado, R.C.P. Rizzo, P.P.S. Peguen, Acta Sci. 26 (2002) 1637.
[33] V.V. Galvita, V.D. Belyaev, V.A. Semikolenov, P. Tsiakaras, A. Frumin, V.A. Sobyanin, React. Kinet. Catal. Lett. 76 (2002) 343.

[34] A. Platon, H.S. Roh, D.L. King, Y. Wang, Top. Catal. 46 (2007) 374.
[35] A. Birot, F. Epron, C. Descorme, D. Duprez, Appl. Catal. B 79 (2008) 17.
[36] W.J. Cai, F.G. Wang, E.S. Zhan, A.C. Van Veen, C. Mirodatos, W.J. Shen, J. Catal. 257 (2008) 96.
[37] M. Domok, K. Baan, T. Kecskes, A. Erdohelyi, Catal. Lett. 126 (2008) 49.
[38] A.C. Bagasiannis, P. Panagiotopoulou, X.E. Verykios, Top. Catal. 51 (2008) 1.
[39] E.I. Santiago, G.A. Camara, E.A. Ticianelli, Electrochim. Acta 48 (2003) 3527.
[40] A. Haryanto, S. Fernando, N. Murali, S. Adhikari, Energy Fuels 19 (2005) 2098.
[41] A. Corma, V. Fornés, S.B. Pergher, Patent EP 9605004 (1996) and WO 9717290 (1997).
[42] A. Corma, A. Martínez, V. Martinez-Soria, J. Catal. 200 (2) (2001) 259.
[43] P. Concepción, C. Lopez, A. Martínez, V.F. Puntes, J. Catal. 228 (2004) 321–332.
[44] A.Y. Khodakov, A. Griboval-Constant, R. Bechara, F. Villain, J. Phys. Chem. B 105 (2001) 9805.
[45] A. Khodakov, A. Griboval-Constant, R. Bechara, V.L. Zholobenko, J. Catal. 206 (2002) 230.
[46] B. Ernst, S. Libs, P. Chaumette, A. Kiennermann, Appl. Catal. A 186 (1999) 145.
[47] A.J. Vizcaíno, A. Carrero, J.A. Calles, Int. J. Hydrogen Energy 32 (2007) 1450–1461.
[48] K. Peng, L. Zhou, A. Hu, Y. Tang, D. Li, Mater. Chem. Phys. 111 (2008) 34–37.
[49] B.D. Cullity, Elements of X-ray Diffraction, Addison–Wesley, London, 1878.
[50] R. Riva, H. Miesner, R. Vitali, G. Del Piero, Appl. Catal. A 196 (2000) 111.
[51] A.Y. Khodakov, J. Lynch, D. Bazin, B. Rebours, N. Zanier, B. Moisson, P. Chaumette, J. Catal. 168 (1997) 16.
[52] D.G. Castner, P.R. Watson, I.Y. Chang, J. Phys. Chem. 94 (1990) 819.
[53] E. van Steen, G.S. Sewell, R.A. Makhothe, C. Micklethwaite, H. Manstein, M. de Lange, C.T. ÓConnor, J. Catal. 162 (1996) 220.
[54] B. Sexton, A. Hughes, T. Turney, J. Catal. 97 (1986) 390.
[55] B. Mile, D. Stirling, M. Zammitt, A. Lovell, M. Webb, J. Catal. 114 (1988) 217.
[56] B. Mile, D. Stirling, M. Zammitt, A. Lovell, M. Webb, J. Mol. Catal. 62 (1988) 179.
[57] A. Diaz, D.R. Acosta, J.A. Odriozola, M. Montes, J. Phys. Chem. B 101 (1997) 1782.
[58] A.J. Akande, R.O. Raphael, A.K. Dalai, Appl. Catal. A 287 (2005) 159–175.